Chemical Methodologies 5 (2021) 522-533

Chemical Methodologies

Journal homepage: http://chemmethod.com

Original Research Article

Photodegradation of Tramadol Using α-Fe_2O_3 nanoparticles/ 12-tungstosilicic Acid as an Efficient Photocatalyst in Water Sample Employing Box-Behnken Design

Farshid Kazemi[1], Hassan Ali Zamani[1,*], Mohammad Reza Abedi[2], Mahmoud Ebrahimi[1]

[1]*Department of Applied Chemistry, Mashhad Branch, Islamic Azad University, Mashhad, Iran*
[2]*Department of Applied Chemistry, Quchan Branch, Islamic Azad University, Quchan, Iran*

ARTICLE INFO

Article history

Submitted: 2021-07-03
Revised: 2021-08-24
Accepted: 2021-10-15
Manuscript ID: CHEMM-2107-1349
Checked for Plagiarism: **Yes**
Language Editor:
Dr. Behrouz Jamalvandi
Editor who approved publication:
Dr. Hamid Reza Arandiyan

DOI: 10.22034/chemm.2021.138835

KEYWORDS

Polyoxometalates
Tramadol
Photodegradation
α-Fe_2O_3 nanoparticles
12-tungstosilicic acid

ABSTRACT

In this study, a photocatalyst based on the combination of a polyoxometalate (12-tungstosilicic acid) and a nanoparticle (α-Fe_2O_3) was prepared to investigate its ability to degrade Tramadol from water samples. The structure, morphology, and functional groups of the synthesized photocatalyst (α-Fe_2O_3/ 12-tungstosilicic acid) were characterized using SEM images, EDX pattern, TEM image, FAM images, and FTIR spectra. Due to the high surface-to-volume ratio in nanoparticles and high intramolecular charge transfer by polyoxometalates, the combination of α-Fe_2O_3 nanoparticles and 12-tungstosilicic acid as a photocatalyst exhibits a high photodegradation efficiency in a suitable time toward the tramadol degradation. Besides, several factors affecting the degradation process of Tramadol with the prepared photocatalyst were evaluated using an experimental design method based on Box-Behnken design to reduce the number of experiments and study the interaction between the factors. In optimal conditions, the tramadol concentration, pH of the sample solution, photocatalyst amount, and the hydrogen peroxide concentration were optimized, which were 90.0 mg L^{-1}, 300 mg L^{-1}, 7.6, and 0.6 mg L^{-1}, respectively. The study of the photocatalyst activity and the degradation kinetics for the tramadol photodegradation as a pharmacological contaminant in a water sample under ultraviolet irradiation exhibited that the synthesized photocatalyst had a high photodegradation efficiency with a pseudo-first-order rate constant of 0.0232 min^{-1} for a photodegradation time of 70 min.

GRAPHICAL ABSTRACT

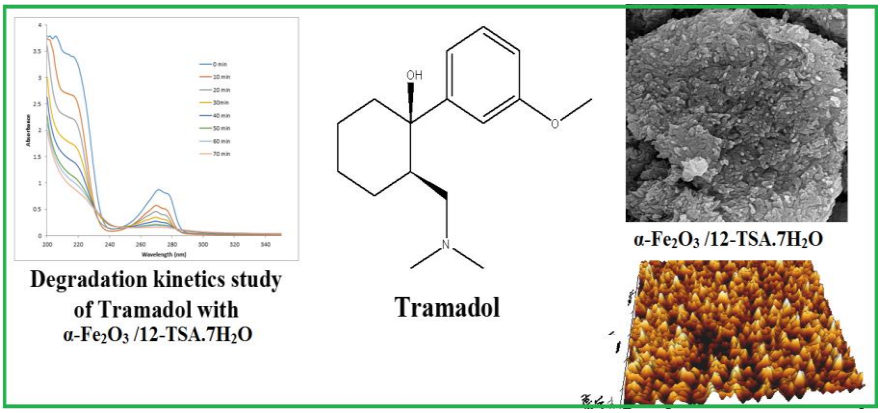

* Corresponding author: Hassan Ali Zamani
✉ E-mail: haszamani93@gmail.com

Introduction

Pharmaceutical compounds have many applications in the treatment of human and animal diseases, leding to the high consumption of these compounds in recent years [1-5]. However, the entry of these drugs through the effluents of pharmaceutical factories causes pollution in water systems [6-10]. Some drug residues taken by patients and metabolites produced in their livers can enter water sources through the house sewage system [11, 12]. The presence of these drugs in water sources can cause serious damage to the environment by entering food chains; as a result, it endangers the health of humans and animals [13-16]. Therefore, the removal of these drugs from water sources has been a major challenge to prevent their adverse effects on the environment.

Various physical and chemical strategies such as flocculation, adsorption, reverse osmosis, coagulation, photodegradation, etc, have been utilized to decrease or remove pollutants from wastewater samples [7,17-19]. The photodegradation procedure requires a heterogeneous or homogenous photocatalyst to remove contaminants even at very low concentrations, which usually do not produce secondary contaminants in the process[20]. Besides, the photodegradation procedure has several advantages, including low cost, low photocatalyst consumption, reusability of photocatalyst, high degradation efficiency, eco-friendliness, and simple operation without the need for sophisticated devices [21, 22]. Several mechanisms were suggested to degrade the organic materials, among which are: a) the formation of the free radicals produced by the electron-hole pairs on the surface of the photocatalyst, and b) the adsorption of the organic materials on the surface of the photocatalyst and reaction with OH radical or the excited electron-hole pairs on the photocatalyst surface [23]. Therefore, the photocatalyst plays an essential role in the success of the pollutant degradation process, which depends on its chemical structure, surface chemical, and physical properties, and surface area [20, 24, 25].

Nanoparticles and nanocomposites are very popular in different industries due to their unique properties such as high surface to volume ratio, the possibility of synthesis by various methods, good thermal, chemical and mechanical stability, and large surface area [26-32]. Nanomaterials have been considered as a unique photocatalyst for the degradation of pollutants owing to their high surface area, the tunability of the surface structure, and the possibility of modifying their surface with suitable functional groups [26, 33-36]. Therefore, the choice of nanomaterial synthesis and its functionalization methods can affect the photocatalyst's ability to degrade contaminants by changing the photocatalyst surface area properties and its energy gap to form electron-hole pairs.

Polyoxometalates (POMs) are nanoclusters of metal oxides with very diverse structures. These various structures of POMs can cause a variety of unique chemical and physical properties in these compounds that led to many applications of these compounds in the fields of photocatalysts, catalysis, sorbents, rechargeable batteries, sensors, fuel cell, and energy storage, etc [37-40]. Due to their high thermal and chemical stability against oxidizing agents, these compounds have been considered as photocatalysts in the presence of oxidizing species such as hydrogen peroxide for the degradation of pollutants [41].

Tramadol is a widely used drug to treat severe pain [42]. It is also known as a serotonin-norepinephrine reuptake inhibitor (SNRIs) drug and is utilized for depression treatment [42, 43]. Tramadol is metabolized in the liver to O-desmethyl Tramadol and *N*-desmethyl Tramadol via the Cytochromes P450 (CYPs) enzymes and excreted in the urine into a household or hospital sewage [44, 45]. Tramadol remains in the water samples due to relatively high solubility in water and negligible volatility of the drug from water samples, which creates the accumulation of the drug in the water source and aquatic organisms [46]. Therefore, it is essential to remove this drug from domestic and hospital effluents before entering the ecosystem to prevent adverse effects on human and animal health.

In a study, a polyoxometalate based on 12-tungstosilicic acid (12-TSA.7H_2O) was synthesized and combined with α-Fe_2O_3 nanoparticles through

a simple and straightforward solid-state synthesis procedure. The ability of α-Fe_2O_3 nanoparticles/12-TSA.7H_2O as a unique photocatalyst for the degradation of Tramadol was investigated under an ultraviolet wave in the presence of hydrogen peroxide. Due to high surface to volume in nanoparticles and high intramolecular charge transfer by polyoxometalates, the combination of a nanoparticle and a polyoxometalate as a proper photocatalyst exhibited a high photodegradation efficiency in a suitable time toward the tramadol degradation. In this study, several factors that affect the Tra degradation process were evaluated and optimized using the experimental design method. The kinetics and activity of the synthesized photocatalyst for the Tra degradation were also investigated, indicating the specific ability of this photocatalyst to degrade Tra in water samples at a pH of about 7.

Material and methods

The materials used to prepare the photocatalyst included sodium tungstate dehydrate (purity ≥ 99 %), sodium silicate solution, iron(III) chloride hexahydrate (purity ≥ 99 %), ethanol (purity ≥ 99.9 %), diethyl ether (purity ≥ 99.7 %), ortho-phosphoric acid solution (purity ≥ 85.0 %), sulfuric acid (purity of 95.0 - 97.0 %), hydrochloric acid (purity 37.0 - 38.0 %), and sodium hydroxide (purity ≥ 97.0 %), which were analytically graded and obtained from Merck (Germany). Tramadol was obtained from Pharma- Chemia Co. (Tehran, Iran).

A UV-Vis spectrophotometer of (Lambda 950, Perkin Elmer, USA) was used to plot the adsorption spectrum of Tramadol in the wavelength range of 200-600 nm and determine the Tramadol concentration. Besides, the Fourier transform infrared spectrophotometer (FTIR, Tensor model, Bruker, Germany), Scanning Electron Microscopy (SEM; Mira 3 Tescan; Czech Republic), Transmission Electron Microscopy (TEM, Philips, CM 120, Netherlands), Atomic Force Microscopy (AFM, JPK. NanoWizard 2, Germany), and X-ray diffraction (XRD, Philips Xpert-pw3040/60, Netherlands) were applied to evaluate the functional groups, structure, and morphology of the synthesized photocatalyst. A pH meter (Metrohm-780, Switzerland) was used to determine and adjust the pH of the water samples.

Synthesis of 12-tungstosilicic acid (12-TSA.7H_2O)

12-tungstosilicic acid was prepared based on previous literature [47]. An aqueous solution (30.0 ml) containing 15.0 g of sodium tungstate dihydrate was added to an aqueous solution of sodium silicate (0.85 mL) with a density of 1.375 g mL^{-1} and stirred for 3 min. The resulting solution was heated to boiling point and concentrated hydrochloric acid (10.0 mL) was added dropwise while stirring for 30 min. After cooling the solution to room temperature, the yellowish-white precipitate was filtered. The concentrated hydrochloric acid (5.0 mL) was added to the supernatant solution and the resulting solution was thoroughly transferred into a separatory funnel. After cooling the solution to room temperature, diethyl ether (12.0 mL) was added to the solution, followed by the solution shaken for 5 min. A three-phase mixture was formed in the funnel with a yellow middle layer. The oily bottom phase was removed and transferred to a new separatory funnel. The solution was shaken again in the funnel and the resulting lower oily phase was separated and added to the previously obtained oily phase. This procedure was repeated several times until the yellow color of the middle phase in the funnel became colorless. Then, 16.0 mL of aqueous hydrochloric acid solution (25 % v/v) and 4.0 mL of diethyl ether were added to the oily phase and shaken for 5 min. A mixture including two phases was formed and the lower phase was carefully separated. To form 12-TSA.7H_2O crystals, the solvent (diethyl ether) was evaporated at room temperature. Finally, the resulting crystals were dried in an oven at 70 °C for 2 h.

Synthesis of α-Fe_2O_3 nanoparticles

An iron (III) chloride hexahydrate solution (0.25 mol L^{-1}, 100.0 mL) was prepared and urea solution (1.0 mol L^{-1}, 100.0 mL) was added to it dropwise for 30 min while stirring vigorously. The resulting solution was stirred for another 30 min and then refluxed at a temperature of 92.5± 2.5 °C for 12 h.

The produced precipitation ($Fe(OH)_3$ with a light brown color) was washed three times with distilled water and dried in an oven at 70 ° C for 2 h. Then, the precipitation was calcined at an electric oven at 300 °C for 1 h to form the dark brown precipitation (α-Fe_2O_3 nanoparticles) [48].

Preparation of α-Fe_2O_3 nanoparticles/ 12-TSA.7H_2O

The photocatalyst was synthesized using the solid-state synthesis method [47]. For this purpose, a mixture of 12-TSA.7H_2O and $Fe(OH)_3$ with a weight ratio of 3 to 1 was poured into a porcelain mortar. The mixture was pulverized using a pestle for 1 h while ethanol as an organic solvent was spared into the mixture. Ethanol spraying was continued until a paste was formed. After mixing with pastels for one hour, the resulting mixture was dried at room temperature and heated in an oven at 80 °C for 1 hour, followed by calcination at 300 °C for 2 h.

Degradation procedure

An aqueous solution of Tramadol (250.0 mL) was poured into a suitable beaker. A suitable amount of photocatalyst and a suitable volume of hydrogen peroxide solution was added to it. The pH of the mixture was adjusted to 7.6 using sodium hydroxide or sulfuric acid solution (0.1 mol L^{-1}). The mixture was stirred for 20 min in the dark to achieve an equilibrium. The resulting mixture was exposed with a UVC lamp (36 W, FPL, 4 pins, Mazda, Japan) at a distance of 20 cm from the surface of the mixture for 20 min while stirring at a rate of 200 rpm. The air in the system was ventilated using a fan during the lamp exposure period to control the temperature in the system. After the exposure time, the photocatalyst was separated from the mixture using a centrifuge at 6000 rpm for 5 min and the concentration of Tramadol in the resulting solution was measured with a UV-Vis spectrophotometer at a wavelength of 272 nm. The photodegradation efficiency was calculated using the following equation 1:

$$PE = \frac{C_i - C_f}{C_i} \times 100 \qquad 1$$

Where PE, C_i, and C_f are the percentage of the photodegradation efficiency, the initial concentration of Tramadol, and the final concentration of Tramadol after the exposure step, respectively.

Result and Dissection

Characterization of the synthesis photocatalyst

SEM image was utilized to evaluate the prepared photocatalyst morphology and structure. SEM images of 12-TSA.7H_2O and α-Fe_2O_3 nanoparticles/ 12-TSA.7H_2O are presented in Figure 1. The SEM image of 12-TSA.7H_2O (Figure 1a) showed that oval particles with irregular sizes in the range of 100-300 nm are formed. Also, the structure of 12-TSA.7H_2O has a suitable and high porosity with irregular and scattered pore size that can be adsorbed the α-Fe_2O_3 nanoparticles and Tra on its surface. According to Figure 1b, the structure of 12-TSA.7H_2O changes during the synthesis of α-Fe_2O_3 nanoparticles/ 12-TSA.7H_2O, which leads to a decrease in particle size (<100 nm) and pore size of the synthesized photocatalyst. There is also an increase in aggregation in the photocatalyst particles, which may be due to the magnetic property and the synthesis condition of α-Fe_2O_3 nanoparticles in the photocatalyst structure [49, 50].

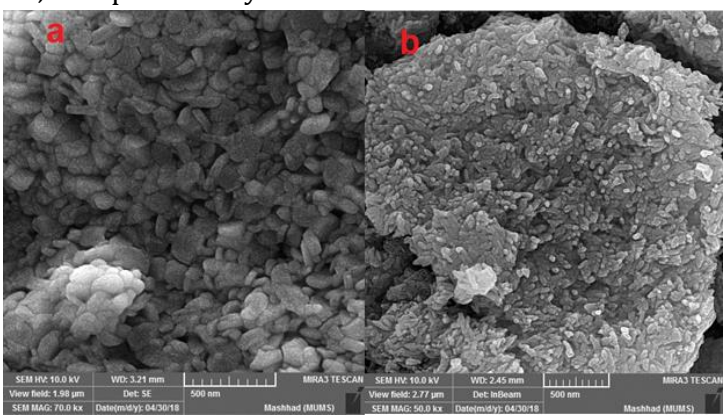

Figure1: SEM image of 12-TSA.7H2O (a) and α-Fe2O3 nanoparticles/ 12-TSA.7H2O (b)

EDX of α-Fe_2O_3 nanoparticles/ 12-TSA.7H_2O is shown in Figure 2, indicating that the important elements on the photocatalyst included silicon, iron, and tungsten in which iron has the highest percentage (93.55 % W) in the structure of the photocatalyst, followed by tungsten with a weight percentage of 4.13 %. The obtained results of EXD are presented in Table S1.

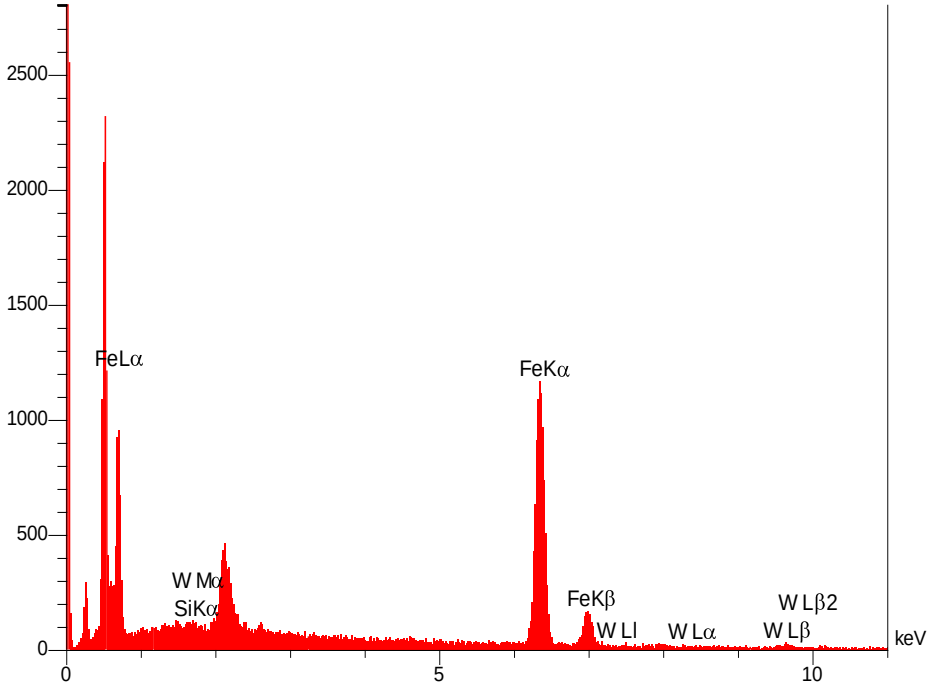

Figure 2: EDX pattern of the α-Fe_2O_3 nanoparticles/ 12-TSA.7H_2O

Examination of the TEM image of α-Fe_2O_3 nanoparticles/ 12-TSA.7H_2O shows that the photocatalyst consists of oval particles with a particle size in the range of 30-70 nm. Also, an aggregation in photocatalytic particles is seen in ESM Figure S1 due to the magnetic properties of α-Fe_2O_3 nanoparticles in the photocatalyst structure.

Atomic force microscopy (AFM) image was applied to analyze the surface topography and thickness of the photocatalyst. The AFM images of α-Fe_2O_3 nanoparticles/ 12-TSA.7H_2O with a scanning area of 3 µm x 3 µm are shown in Figure 3. As can be seen in Figures 3a and b, the photocatalyst has a non-uniform surface that leads to adsorb Tra with high efficiency in the photocatalyst surface pores. The root mean square (RMS) value for the α-Fe_2O_3 nanoparticles/ 12-TSA.7H_2O was found to be 2.502 nm, indicating the photocatalyst has a low superficial roughness with a smooth surface.

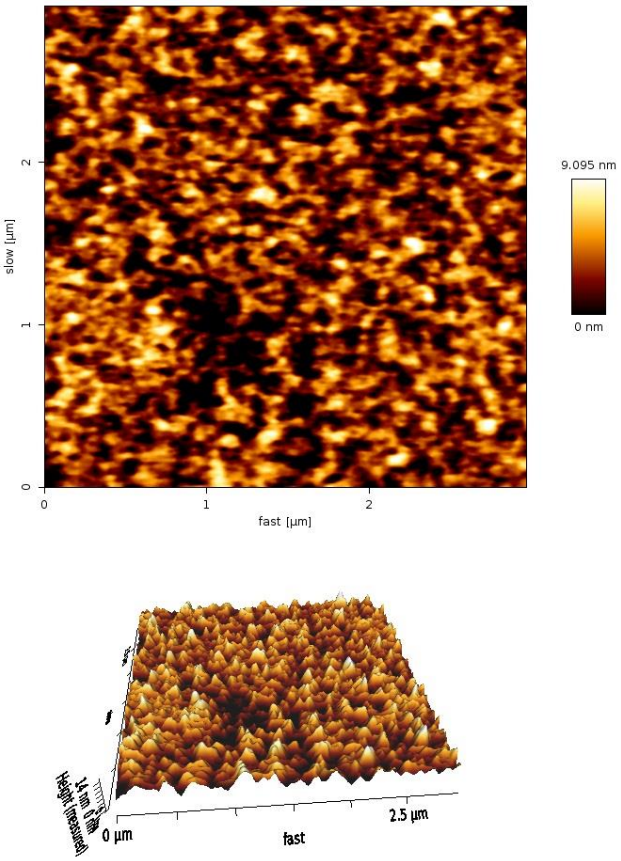

Figure 3: AFM image of the α-Fe_2O_3 nanoparticles/ 12-TSA.7H_2O

FTIR images of the α-Fe_2O_3 nanoparticles and α-Fe_2O_3 nanoparticles/ 12-TSA.7H_2O are presented in Figures 4a and b, respectively, in which the absorption peak at 582.32 Cm^{-1} is related to the Fe-O group on the α-Fe_2O_3 nanoparticles that shifted to 534.51 Cm^{-1} in the photocatalyst. An antisymmetric stretching vibration peak at 981.43 Cm^{-1} corresponded to Si-O-Si functional groups in 12-TSA.7H_2O. Also, two vibration peaks at 922.77 and 789.31 Cm^{-1} are related to the stretching vibration of the W-O group and the antisymmetric stretching vibration of the W-O-W group in 12-TSA.7H_2O, respectively. The peaks at 1621 Cm^{-1} and 1624 Cm^{-1} are related to the bending vibration of OH in the α-Fe_2O_3 nanoparticles and α-Fe_2O_3 nanoparticles/ 12-TSA.7H_2O, respectively [48]. The broad peaks at 3426.32 and 3418.05 Cm^{-1} may be due to adsorbing the water molecular in the network structure of α-Fe_2O_3 nanoparticles and α-Fe_2O_3 nanoparticles/ 12-TSA.7H_2O, respectively.

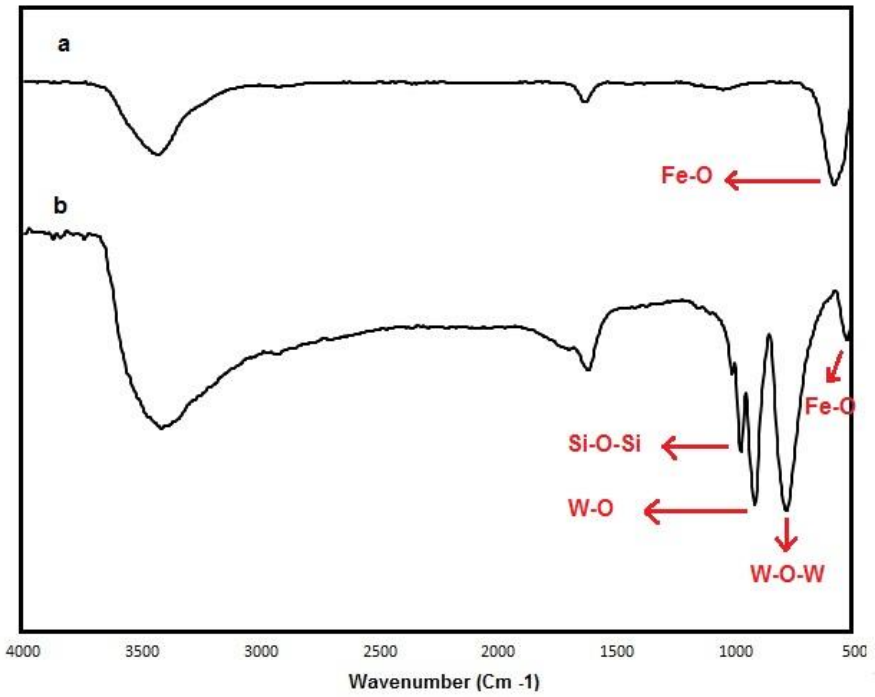

Figure 4: FTIR spectra of the α-Fe_2O_3 nanoparticles (a) and the α-Fe_2O_3 nanoparticles/ 12-TSA.7H_2O (b)

Optimization of photodegradation procedure

The photodegradation process is deponed on various parameters that controlling and optimizing them can greatly increase the degradation efficiency of pollution. Therefore, several factors such as the Tra concentration, pH of the sample solution, photocatalyst amount, and the hydrogen peroxide amount may affect the Tra degradation and so the effectiveness of these factors was evaluated on the degradation efficiency of Tra using an experimental design. For this purpose, a Box-Behnken design including 27 experimental runs was created for the optimization of these factors. The experiments provided by the Box-Behnken design were performed in a random order to eliminate the effects of uncontrollable factors. The selected factors and their levels are shown in Table 1.

Table 1: Factors and selected levels for the optimization of the photocatalytic procedure.

Factor	Symbol	Level		
		Low	Center	High
Tra concentration (mg L^{-1})	A	90	130	170
Photocatalyst amount (mg L^{-1})	B	100	200	300
pH of the sample solution	C	5.0	6.5	8.0
H_2O_2 concentration (Mol L^{-1})	D	0.2	0.4	0.6

Besides, the experimental runs and the photodegradation efficiency percentage of Tra with each run are presented in Table 2. Each experiment in Table 2 was repeated three times under the same conditions, and the mean degradation efficiency of Tra obtained for the three replications of the experiment was considered as the response (PE%) in Table 2.

Table 2: The Box-Behnken design for the optimization of the photocatalytic procedure

Std Order	Run Order	Pt Type	Blocks	A	B	C	D	PE% ± S
21	1	2	1	130	100	6.5	0.2	65.23 ± 0.53
18	2	2	1	170	200	5.0	0.4	54.19 ± 0.58
1	3	2	1	90	100	6.5	0.4	80.13 ± 0.63
13	4	2	1	130	100	5.0	0.4	60.31 ± 0.59
20	5	2	1	170	200	8.0	0.4	59.02 ± 0.54
5	6	2	1	130	200	5.0	0.2	64.51 ± 0.66
17	7	2	1	90	200	5.0	0.4	77.17 ± 0.71
7	8	2	1	130	200	5.0	0.6	69.13 ± 0.53
10	9	2	1	170	200	6.5	0.2	59.49 ± 0.67
14	10	2	1	130	300	5.0	0.4	70.11 ± 0.64
2	11	2	1	170	100	6.5	0.4	56.17 ± 0.51
4	12	2	1	170	300	6.5	0.4	62.44 ± 0.63
27	13	0	1	130	200	6.5	0.4	73.18 ± 0.76
3	14	2	1	90	300	6.5	0.4	93.55 ± 0.59
11	15	2	1	90	200	6.5	0.6	89.83 ± 0.66
23	16	2	1	130	100	6.5	0.6	70.71 ± 0.73
22	17	2	1	130	300	6.5	0.2	78.13 ± 0.64
12	18	2	1	170	200	6.5	0.6	55.19 ± 0.58
16	19	2	1	130	300	8.0	0.4	79.93 ± 0.61
15	20	2	1	130	100	8.0	0.4	68.14 ± 0. 53
6	21	2	1	130	200	8.0	0.2	73.44 ± 0.62
26	22	0	1	130	200	6.5	0.4	77.11 ± 0.70
9	23	2	1	90	200	6.5	0.2	80.62 ± 0.65
8	24	2	1	130	200	8.0	0.6	78.19 ± 0.59
24	25	2	1	130	300	6.5	0.6	80.37 ± 0.73
19	26	2	1	90	200	8.0	0.4	85.44 ± 0.56
25	27	0	1	130	200	6.5	0.4	74.51 ± 0.61

One-way analysis of variance (One-way ANOVA) as a suitable statistical test at a 95% confidence level was utilized to investigate the effects of the factors and their interactions (Table 3). P-value is a proper parameter in the ANOVA Table that can be applied to evaluate the significance of the factors and their interactions. A factor or an interaction is a significant independent variable with a p-value of less than 0.05 at a 95% confidence level. In other words, factors or interactions with a p-value greater than 0.05 are known as nonsignificant factors in the Tra degradation efficiency. According to Table 3, all four studied factors have a significant effect on the Tra degradation efficiency because their p-value is less than 0.05. Besides, evaluation of the interaction between the factors shows that all interactions between the factors have not a significant effect on the Tra degradation efficiency. Only the interaction between the concentration of Tra and the concentration of hydrogen peroxide (AD) have a significant effect on the Tra degradation efficiency at a 95% confidence level with a value of 0.002 (p-value<0.05). The p-value can also be applied to investigate the provided model by the Box-Behnken design. The p-value of the model presented for the Tra degradation is lower than 0.05, indicating that the model was fitted well with the obtained responses (PE%). Another suitable parameter for evaluating the model presented by the Box - Benken design is Lack of Fit (LOF). A model is presented with well-fitted results when LOF is a meaningless parameter with a p-value greater than 0.05. Therefore, a p-value of 0.743 (p-value>0.05) obtained for LOF indicates that this parameter is

nonsignificant and the model fits well with the responses (PE%). However, the proposed model can be described by a quadratic equation. This equation shows the relationship between the effect of factors and interactions on the Tra degradation efficiency. The quadratic equation obtained in the design of the Box - Benken design for the Tra degradation is as follows equation 2:

Table 3: Analysis of variance for the optimization of the photocatalytic procedure

Source	DF	Adj SS	Adj MS	F-Value	P-Value
Model	14	2872.67	205.19	73.32	0.000
Linear	4	2717.67	679.42	242.77	0.000
A	1	2139.74	2139.74	764.59	0.000
B	1	339.63	339.63	121.36	0.000
C	1	197.97	197.97	70.74	0.000
D	1	40.33	40.33	14.41	0.003
Square	4	90.02	22.50	8.04	0.002
A*A	1	24.01	24.01	8.58	0.013
B*B	1	2.08	2.08	0.74	0.406
C*C	1	78.20	78.20	27.94	0.000
D*D	1	2.41	2.41	0.86	0.372
2-Way Interaction	6	64.99	10.83	3.87	0.022
A*B	1	12.78	12.78	4.57	0.054
A*C	1	2.96	2.96	1.06	0.324
A*D	1	45.63	45.63	16.30	0.002
B*C	1	0.99	0.99	0.35	0.563
B*D	1	2.62	2.62	0.94	0.352
C*D	1	0.00	0.00	0.00	0.970
Error	12	33.58	2.80		
Lack-of-Fit	10	25.59	2.56	0.64	0.743
Pure Error	2	7.99	4.00		
Total	26	2906.25			

$$PE\% = -57.4 + 0.362\ A + 0.1309\ B + 25.99\ C + 84.9\ D - 0.001326\ A*A - 0.000062\ B*B - 1.702\ C*C - 16.8\ D*D - 0.000447\ A*B - 0.0143\ A*C - 0.422\ A*D + 0.00332\ B*C - 0.0405\ B*D + 0.11\ C*D \quad (2)$$

The obtained quadratic equation can show the relationship between factors and interactions with the Tra degradation efficiency (PE%) because the values of R-squared and adjusted R-squared of the equation are equal to 98.84 and 97.50%, respectively. Also, a high predicted R-squared (94.31%) indicates that the obtained equation can be well utilized to predict the Tra degradation efficiency theoretically. According to Equation 2, the hydrogen peroxide concentration (D) is the critical factor with a positive effect on the Tra degradation efficiency (PE%) because its regression coefficient in Eq. 2 is the highest. The next important factor with a positive effect on the Tra degradation efficiency (PE%) is the pH of the sample solution (C) with a positive regression coefficient of 25.99 in Eq. 2. The most important interaction with a negative effect is the interaction between Tra concentration and hydrogen peroxide concentration (AD) with a negative regression coefficient of 0.422. The effect of factors is higher than the effects of their interaction because of a higher regression coefficient of factors than the regression coefficient of interactions. The surface and contour plots of the critical interaction (AD) are presented in Figure S2, indicating that the Tra degradation efficiency (PE%) was increased by decreasing the Tra concentration and increasing the hydrogen peroxide concentration simultaneously. Obviously, the Tera degradation efficiency increases with increasing concentration of hydrogen peroxide as an oxidizing agent.

The optimization plot for Tra degradation efficiency with the prepared photocatalyst is shown in Figure S3. Therefore, the optimum amount of Tra concentration (A), photocatalyst amount (B), pH of sample solution (C), and hydrogen peroxide concentration (D) was 90.0 mg L^{-1}, 300 mg L^{-1}, 7.6, and 0.6 mg L^{-1}, respectively.

Kinetic of photocatalytic degradation

The activity of the prepared photocatalyst for degradation of the Tra residues as a pharmacological contaminant in a water sample was studied under ultraviolet irradiation by a UVC lamp (36 W, FPL, 4 pins, Mazda, Japan). The photocatalyst amount and concentration of Tra for the study were 300 mg L^{-1} and 130.0 mg L^{-1}, respectively. After achieving an absorption-desorption equilibration between the photocatalyst and sample solution for 20 min in the dark, the degradation procedure under UV exposure was performed at intervals of 0-70 min at room temperature under stirring at 200 rpm. The sampling of the study solution was performed every 10 min from the start of exposure with a 2 ml pipette while stirring and exposure were stopped. The obtained samples were analyzed to determine the Tra concentration after centrifugation of the sample for 3 min at 600 rpm to ensure complete removal of the photocatalyst before Tra measurement. The degradation efficiency of Tra was also determined by Eq. 1. The spectrophotometric spectra of Tra in times of 10 to 70 minutes are shown in ESM Figure S4, indicating that the Tra absorbance decreases greatly with increasing the degradation time up to 60 min at the maximum absorption wavelength of Tra (272 nm). Besides, there is no change in the shape of the Tra absorption peak; only a decrease in the severity of absorbance occurs with increasing the degradation time in the presence of the photocatalyst. However, metal atoms in the polyoxometalates such as tungsten (W^{6+}) in the 12-TSA.$7H_2O$ network are generally full oxidization with a d^0 electronic configuration that can display a suitable charge transfer between ligand to metal (LMCT) through charge transfer O^{2-} ($2p^6$) to W^{6+} ($5d^0$) to form the photoexcited states through the intramolecular charge transfer between HOMO orbital of O^{2-} and LUMO orbital of W^{6+}[42]. As a result, the photoexcited 12-TSA.$7H_2O$ is highly active to perform the photocatalytic degradation of Tra in the presence of hydrogen peroxide as an oxidizing agent. Thus, the highest degradation of Tra is founded for the α-Fe_2O_3 nanoparticles/12-TSA.$7H_2O$ at a time of about 70 min.

The degradation kinetics study of Tra was evaluated using the α-Fe_2O_3 nanoparticles/12-TSA.$7H_2O$ as a photocatalyst under the optimum conditions with the Langmuir-Hinshelwood model. For this purpose, the pseudo-first-order rate constant as a critical parameter was determined at different times from 10 to 70 min by plotting the first-order rate curve based on the following equation 3 [51]:

$$-ln\left(\frac{C}{C_0}\right) = Kt \qquad 3$$

where k, C_o, and C are the pseudo-first-order rate constant, the Tra concentration (t=0), and the Tra concentration at time equal to t (t=10-70 min), respectively. A rate constant (k) of Tra degradation of 0.0232 min^{-1} with a determination coefficient (R^2) 0.9656 is calculated for the α-Fe_2O_3 nanoparticles/12-TSA.$7H_2O$ as a photocatalyst, indicating that the Tra degradation was carried out with a suitable rate and the prepared photocatalyst had a high ability to degrade Tra from water sample with a suitable degradation efficiency at a proper time (Figure 5).

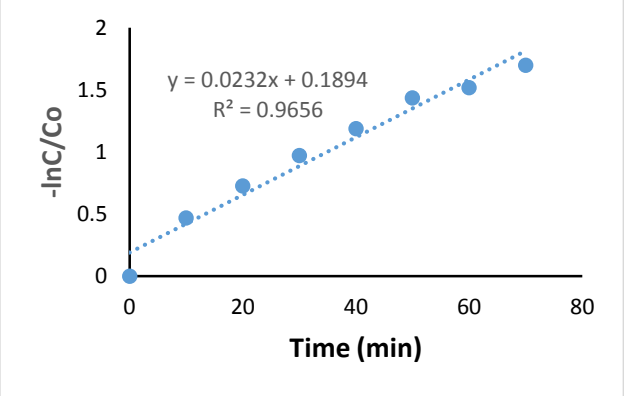

Figure 5: The degradation kinetics study of Tra using the α-Fe_2O_3 nanoparticles/12-TSA.$7H_2O$ as a photocatalyst

Conclusion

Polyoxometalate as a photocatalyst has a suitable ability to degrade pollution in water samples. Therefore, 12-tungstosilicic acid (12-TSA.$7H_2O$) was chemically synthesized as a compound from the class of polyoxometalate and combined with α-Fe_2O_3 nanoparticles through a simple and straightforward solid-state synthesis method. The prepared photocatalyst (α-Fe_2O_3 nanoparticles/12-TSA.$7H_2O$) displayed a unique

ability for the degradation of an analgesic and antidepressant drug (Tramadol) under an ultraviolet wave in the presence of hydrogen peroxide. The high photodegradation efficiency of Tramadol using α-Fe_2O_3 nanoparticles/12-TSA.$7H_2O$ as a photocatalyst is due to the unique properties of α-Fe_2O_3 nanoparticles such as a high surface to volume ratio and adsorption capacity and excellent properties of 12-TSA.$7H_2O$, including a high intramolecular charge transfer. The effective factors in the tramadol degradation with α-Fe_2O_3 nanoparticles/12-TSA.$7H_2O$ as a photocatalyst was performed by an experimental design including Box-Behnken design with 27 experimental runs. The optimum amount of Tra concentration, photocatalyst amount, pH of sample solution, and hydrogen peroxide concentration was 90.0 mg L^{-1}, 300 mg L^{-1}, 7.6, and 0.6 mg L^{-1}, respectively. Factor optimization showed that the degradation process of Tramadol performed well under mild conditions such as pH 7.6, and hydrogen peroxide concentration of 0.6 mg L^{-1} under ultraviolet light. The kinetics and activity of the synthesized photocatalyst for the tramadol degradation were also investigated, indicating the specific ability of this photocatalyst to degrade Tramadol in water samples at a pH of 7.6 with a first-order rate constant (k) of Tra degradation of 0.0232 min^{-1} and a determination coefficient (R^2) 0.9656 for 70 min. The advantages of the photocatalyst to degrade Tramadol included high photodegradation efficiency, suitable degradation time and proper activity under mild degradation condition.

Acknowledgments

The Azad University of Mashhad, Iran, and the Azad University of Quchan, Iran are appreciated for their support.

Funding

This research did not receive any specific grant from funding agencies in the public, commercial, or not-for-profit sectors.

Authors' contributions

All authors contributed toward data analysis, drafting and revising the paper and agreed to be responsible for all the aspects of this work.

Conflict of Interest

We have no conflicts of interest to disclose.

References

[1]. Sinha N.A., Kumar V., *Measurement, Analysis and Remediation of Environmental Pollutants*, Springer, 2020 [Crossref], [Google Scholar], [Publisher]

[2]. Karimi-Maleh H., Ayati A., Davoodi R., Tanhaei B., Karimi F., Malekmohammadi S., Orooji Y., Fu L., Sillanpää M., *J. Clean. Prod.,* 2021, **291**:125880 [Crossref], [Google Scholar], [Publisher]

[3]. Karaman C., Karaman O., Atar N., Yola M.L., *Microchim. Acta,* 2021, **188**:1 [Crossref], [Google Scholar], [Publisher]

[4]. Karaman C., Karaman O., Yola B.B., Ulker İ., Atar N., Yola M.L., *New J. Chem.,* 2021, **45**:11222 [Crossref], [Google Scholar], [Publisher]

[5]. Karimi-Maleh H., Cellat K., Arıkan K., Savk A., Karimi F., Şen F., *Mater. Chem. Phys.,* 2020, **250**:123042 [Crossref], [Google Scholar], [Publisher]

[6]. Kalyva M., 2017, [Google Scholar], [Publisher]

[7]. Gordi Z., Ghorbani M., Ahmadian Khakhiyani M., *Water Environ. Res.,* 2020, **92**:1935 [Crossref], [Google Scholar], [Publisher]

[8]. Lübbert C., Baars C., Dayakar A., Lippmann N., Rodloff A.C., Kinzig M., Sörgel F., *Infection,* 2017, **45**: 479 [Crossref], [Google Scholar], [Publisher]

[9]. Ghorbani M., Aghamohammadhasan M., Shams A., Tajfirooz F., Pourhassan R., Khosravi S.R.B., Karimi E., Jampour A., *Microchem. J.,* 2018, **145**:1026 [Crossref], [Google Scholar], [Publisher]

[10]. Ghorbani M., Chamsaz M., Aghamohammadhasan M., Shams A., *Anal. Biochem.,* 2018, **551**:7 [Crossref], [Google Scholar], [Publisher]

[11]. Dogan A., Płotka-Wasylka J., Kempińska-Kupczyk D., Namieśnik J., Kot-Wasik A., *TrAC Trends Anal. Chem.,* 2020, **122**:115710 [Crossref], [Google Scholar], [Publisher]

[12]. Depaolini A.R., Fattore E., Cappelli F., Pellegrino R., Castiglioni S., Zuccato E., Fanelli R., Davoli E., *J. Chromatogr. B,* 2016, **1023**:62 [Crossref], [Google Scholar], [Publisher]

[13]. Mackuľak T., Černanský S., Fehér M., Birošová L., Gál M., *Curr. Opin. Environ. Sci. Health,*

2019, **9**:40 [Crossref], [Google Scholar], [Publisher]
[14]. Ghorbani M., Chamsaz M., Rounaghi G.H., *Anal. Bioanal. Chem.,* 2016, **408**:4247 [Crossref], [Google Scholar], [Publisher]
[15]. Ghorbani M., Chamsaz M., Rounaghi G.H., *J. Sep. Sci.,* 2016, **39**:1082 [Crossref], [Google Scholar], [Publisher]
[16]. Ghorbani M., Esmaelnia M., Aghamohammadhasan M., Akhlaghi H., Seyedin O., Azari Z.A., *J. Anal. Chem.,* 2019, **74**:540 [Crossref], [Google Scholar], [Publisher]
[17]. Jagaba A., Kutty S., Hayder G., Baloo L., Ghaleb A., Lawal I., Abubakar S., Al-dhawi B., Almahbashi N., Umaru I., *Ain Shams Eng. J.,* 2020, **12**:57 [Crossref], [Google Scholar], [Publisher]
[18]. Zhao C., Zhou J., Yan Y., Yang L., Xing G., Li H., Wu P., Wang M., Zheng H., *Sci. Total Environ.,* 2020, **199**:142795 [Crossref], [Google Scholar], [Publisher]
[19]. Ghorbani M., Seyedin O., Aghamohammadhassan M., *J. Environ. Manag.,* 2020, **254**:109814 [Crossref], [Google Scholar], [Publisher]
[20]. Kumar A., Pandey G., *Mater. Sci. Eng. Int. J,* 2017, **1**:1 [Google Scholar]
[21]. Kumar S., Ahlawat W., Bhanjana G., Heydarifard S., Nazhad M.M., Dilbaghi N., *J. Nanosci. Nanotechnol.,* 2014, **14**:1838 [Crossref], [Google Scholar], [Publisher]
[22]. Szczepanik B., *Appl. Clay Sci.,* 2017, **141**:227 [Crossref], [Google Scholar], [Publisher]
[23]. Santhosh C., Velmurugan V., Jacob G., Jeong S.K., Grace A.N., Bhatnagar A., *Chem. Eng. J.,* 2016, **306**:1116 [Crossref], [Google Scholar], [Publisher]
[24]. Zou W., Gao B., Ok Y.S., Dong L., *Chemosphere,* 2019, **218**: 845 [Crossref], [Google Scholar], [Publisher]
[25]. Reza K.M., Kurny A., Gulshan F., *Appl. Water Sci.,* 2017, **7**:1569 [Crossref], [Google Scholar], [Publisher]
[26]. Joy J., Mathew J., George S.C., *Int. J. Hydrog Energy,* 2018, **43**:4804 [Crossref], [Google Scholar], [Publisher]
[27]. Miraki M., Karimi-Maleh H., Taher M.A., Cheraghi S., Karimi F., Agarwal S., Gupta V.K., *J. Mol. Liq.,* 2019, **278**:672 [Crossref], [Google Scholar], [Publisher]
[28]. Akça A., Karaman O., Karaman C., *ECS J. Solid State. Sci. Technol.,* 2021, **10**:041003 [Google Scholar], [Publisher]
[29]. Karimi-Maleh H., Sheikhshoaie M., Sheikhshoaie I., Ranjbar M., Alizadeh J., Maxakato N.W., Abbaspourrad A., *New J. Chem.,* 2019, **43**:2362 [Crossref], [Google Scholar], [Publisher]
[30]. Ghorbani M., Ariavand S., Aghamohammadhasan M., Seyedin O., *J. Iran. Chem. Soc.,* 2021, **18**:1947 [Crossref], [Google Scholar], [Publisher]
[31]. Mohammadi P., Ghorbani M., Mohammadi P., Keshavarzi M., Rastegar A., Aghamohammadhassan M., Saghafi A., *Microchem. J.,* 2021, **160**:105680 [Crossref], [Google Scholar], [Publisher]
[32]. Ghorbani M., Mohammadi P., Keshavarzi M., Saghi M.H., Mohammadi M., Shams A., Aghamohammadhasan M., *Anal. Chimica Acta,* 2021, **1178**:338802 [Crossref], [Google Scholar], [Publisher]
[33]. Khalid N., Majid A., Tahir M.B., Niaz N., Khalid S., *Ceram. Int.,* 2017, **43**:14552 [Crossref], [Google Scholar], [Publisher]
[34]. Bethi B., Sonawane S.H., Bhanvase B.A., Gumfekar S.P., *Chem. Eng. Process.,* 2016, **109**:178 [Crossref], [Google Scholar], [Publisher]
[35]. Karimi-Maleh H., Kumar B.G., Rajendran S., Qin J., Vadivel S., Durgalakshmi D., Gracia F., Soto-Moscoso M., Orooji Y., Karimi F., *J. Mol. Liq.,* 2020, **314**:113588 [Crossref], [Google Scholar], [Publisher]
[36]. Orooji Y., Tanhaei B., Ayati A., Tabrizi S.H., Alizadeh M., Bamoharram F.F., Karimi F., Salmanpour S., Rouhi J., Afshar S., *Chemosphere,* 2021, **281**:130795 [Crossref], [Google Scholar], [Publisher]
[37]. Huang B., Yang D.-H., Han B.-H., *J. Mater. Chem. A,* 2020, **8**:4593 [Crossref], [Google Scholar], [Publisher]
[38]. Stamate A.-E., Pavel O.D., Zavoianu R., Marcu I.-C., *Catalysts,* 2020, **10**:57 [Crossref], [Google Scholar], [Publisher]
[39]. Zhai L., Li H., *Molecules,* 2019, **24**:3425 [Crossref], [Google Scholar], [Publisher]
[40]. Chen J.J.J., Barteau M.A., *J. Energy Storage,* 2017, **13**:255 [Crossref], [Google Scholar], [Publisher]

[41]. Suzuki K., Mizuno N., Yamaguchi K., *ACS Catalysis,* 2018, **8**:10809 [Crossref], [Google Scholar], [Publisher]
[42]. Kaye A.D., *Pain Physician,* 2015, **18**:395 [Google Scholar]
[43]. Bloms-Funke P., Dremencov E., Cremers T., Tzschentke T., *Neurosci. Lett.,* 2011, **490**:191 [Crossref], [Google Scholar], [Publisher]
[44]. Allegaert K., Holford N., Anderson B.J., Holford S., Stuber F., Rochette A., Trocóniz I.F., Beier H., de Hoon J.N., Pedersen R.S., *Clin. Pharmacokinet,* 2015, **54**:167 [Crossref], [Google Scholar], [Publisher]
[45]. Samer C.F., Lorenzini K.I., Rollason V., Daali Y., Desmeules J.A., *Mol. Diagn. Ther.*, 2013, **17**:165 [Crossref], [Google Scholar], [Publisher]
[46]. Rúa-Gómez P.C., Püttmann W., *Environ. Sci. Pollut. Res.,* 2012, **19**:689 [Crossref], [Google Scholar], [Publisher]
[47]. Saghi M., Mahanpoor K., Shafiei H., *Iran. J. Chem. Chem. Eng.,* 2018, **37**:1 [Crossref], [Google Scholar], [Publisher]
[48]. Bharathi S., Nataraj D., Mangalaraj D., Masuda Y., Senthil K., Yong K., *J. Phys. D Appl. Phys*., 2009, **43**:015501 [Google Scholar], [Publisher]
[49]. Frandsen C., Mørup S., *J. Condens. Matter Phys.,* 2006, **18**: 7079 [Google Scholar], [Publisher]
[50]. Liu Z., Cheng Q., Wang Y., Zheng A., Li K., Zhang J., *Chem. Phys. Lett.,* 2020, **760**:137901 [Crossref], [Google Scholar], [Publisher]
[51]. Khoshnood R.S., Khoshnoud D.S., *Appl. Phys. A,* 2019, **125**:750 [Crossref], [Google Scholar], [Publisher]

HOW TO CITE THIS ARTICLE
Farshid Kazemi, Hassan Ali Zamani, Mohammad Reza Abedi, Mahmoud Ebrahimi. Photodegradation of Tramadol Using α-Fe_2O_3 nanoparticles/ 12-tungstosilicic Acid as an Efficient Photocatalyst in Water Sample Employing Box-Behnken Design, Chem. Methodol., 2021, 5(6) 522-533
DOI: 10.22034/chemm.2021.138835
URL: http://www.chemmethod.com/article_138835.html